Reiss, M. C., Rümpker, G., Tilmann, F., Yuan, X., Giese, J., Rindraharisaona, E. J. (2016): Seismic anisotropy of the lithosphere and asthenosphere beneath southern Madagascar from teleseismic shear wave splitting analysis and waveform modeling. - *Journal of Geophysical Research*, *121*, 9, pp. 6627—6643.

DOI: http://doi.org/10.1002/2016JB013020

AGU PUBLICATIONS

JGR

Journal of Geophysical Research: Solid Earth

RESEARCH ARTICLE
10.1002/2016JB013020

Key Points:
- Fast polarization directions rotate from NW in the center to NE in the east and west of southern Madagascar
- Results are best explained by the alignment of olivine fast axes parallel to APM in the asthenosphere and variable crustal anisotropy
- Crustal anisotropy is interpreted as being caused by a zone of ductile deformation

Supporting Information:
- Supporting information S1

Correspondence to:
M. C. Reiss,
reiss@geophysik.uni-frankfurt.de

Citation:
Reiss, M. C., G. Rümpker, F. Tilmann, X. Yuan, J. Giese, and E. J. Rindraharisaona (2016), Seismic anisotropy of the lithosphere and asthenosphere beneath southern Madagascar from teleseismic shear wave splitting analysis and waveform modeling, *J. Geophys. Res. Solid Earth*, *121*, 6627–6643, doi:10.1002/2016JB013020.

Received 24 MAR 2016
Accepted 24 AUG 2016
Accepted article online 26 AUG 2016
Published online 17 SEP 2016

Seismic anisotropy of the lithosphere and asthenosphere beneath southern Madagascar from teleseismic shear wave splitting analysis and waveform modeling

M. C. Reiss[1], G. Rümpker[1], F. Tilmann[2,3], X. Yuan[2], J. Giese[3], and E. J. Rindraharisaona[2,4]

[1]Institute of Geosciences, Goethe University Frankfurt, Frankfurt am Main, Germany, [2]GFZ German Research Centre for Geosciences, Potsdam, Germany, [3]Department of Earth Sciences, Institute of Geological Sciences, Tectonics and Sedimentary Geology, Freie Universität Berlin, Berlin, Germany, [4]Institute and Observatory of Geophysics Antananarivo, Antananarivo, Madagascar

Abstract Madagascar occupies a key position in the assembly and breakup of the supercontinent Gondwana. It has been used in numerous geological studies to reconstruct its original position within Gondwana and to derive plate kinematics. Seismological observations in Madagascar to date have been sparse. Using a temporary, dense seismic profile across southern Madagascar, we present the first published study of seismic anisotropy from shear wave splitting analyses of teleseismic phases. The splitting parameters obtained show significant small-scale variation of fast polarization directions and delay times across the profile, with fast polarization rotating from NW in the center to NE in the east and west of the profile. The delay times range between 0.4 and 1.5 s. A joint inversion of waveforms at each station is applied to derive hypothetical one-layer splitting parameters. We use finite-difference, full-waveform modeling to test several hypotheses about the origin and extent of seismic anisotropy. Our observations can be explained by asthenospheric anisotropy with a fast polarization direction of 50°, approximately parallel to the absolute plate motion direction, in combination with blocks of crustal anisotropy. Predictions of seismic anisotropy as inferred from global mantle flow models or global anisotropic surface wave tomography are not in agreement with the observations. Small-scale variations of splitting parameters require significant crustal anisotropy. Considering the complex geology of Madagascar, we interpret the change in fast-axis directions as a ~150 km wide zone of ductile deformation in the crust as a result of the intense reworking of lithospheric material during the Pan-African orogeny. This fossil anisotropic pattern is underlain by asthenospheric anisotropy induced by plate motion.

1. Introduction

As many crustal and mantle materials will align in response to the strain they experienced, the past and present kinematics of the Earth's interior can be studied by the analysis of shear wave splitting, caused by seismic anisotropy, which, in turn, provides important constraints on dynamic processes. A shear wave traveling through an anisotropic medium is split into two orthogonally polarized fast and slow wave components. The extent and strength of anisotropy affect the delay time δt between the two components, and the orientation of the fast axis of the anisotropic layer ϕ is derived from the polarization of the fast shear wave. Two different mechanisms are usually invoked to explain seismic anisotropy: the first is crystallographic preferred orientation (CPO) of minerals due to strain induced by flow [e.g., *Long and Silver*, 2009; *Savage*, 1999], e.g., the alignment of the fast axis of olivine in the direction of shear through dislocation creep [e.g., *Karato and Wu*, 1993]. However, CPO also occurs frequently in middle and lower crustal rocks [*Okaya et al.*, 1995; *Ko and Jung*, 2015]. The second mechanism is shape-preferred orientation (SPO) due to aligned inclusions such as fluid-filled cracks in the crust [*Crampin et al.*, 1984] or melt-filled lenses in the mantle [e.g., *Holtzman and Kendall*, 2010; *Walker et al.*, 2004].

In ocean basins, shear wave splitting results are mostly interpreted in terms of seismic anisotropy due to crystallographic preferred orientation (CPO) caused by simple shear in the asthenosphere, which accommodates the movement of the rigid lithosphere and upper mantle flow resulting in fast directions approximately aligned with the absolute plate motion (APM) directions; for old ocean basins, the effects of frozen fossil spreading directions are preserved in the lithosphere [e.g., *Savage*, 1999; *Long and Silver*, 2009]. Comparisons between shear wave splitting observations and predictions of anisotropy due to mantle flow

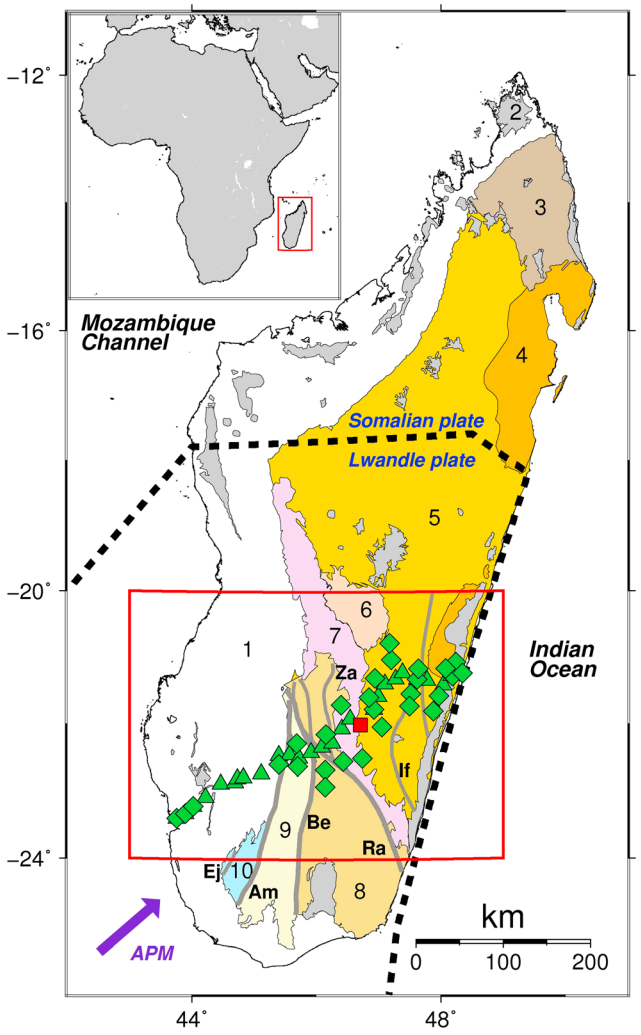

Figure 1. Simplified geological map of Madagascar after *Bésairie* [1971], *Jourde* [1971], and *Collins* [2000]. 1, Sediments; 2, volcanic formations; 3, Bemarivo orogenic belt; 4, Antongil Block; 5, Antananarivo Block; 6, Itremo sheet; 7, Ikalamavony Domain; 8, Anosyen Domain; 9, Androyen Domain; and 10, Vohibory Domain. Grey lines are shear zones modified after *Martelat et al.* [2000] Ej, Ejeda; Am, Ampanihy; Be, Beraketa; Ra, Ranotsara; Za, Zazafotsy; and If, Ifanadiana. Dashed black line is the proposed plate boundary between the Lwandle plate and Somalian plate [*Stamps et al.*, 2014]. Red frame marks the research area shown in Figures 5 and 6. Green triangles show broadband stations, green diamonds denote short-period stations, and the red square marks the permanent station VOI of the GEOFON network.

from geodynamic models show a substantial correlation [e.g., *Becker et al.*, 2014]. However, beneath continents with their often complex geological history, the study of shear wave splitting often reveals smaller-scale variations, which cannot easily be attributed to a single source, although the same fundamental mechanisms are at play [e.g., *Fouch and Rondenay*, 2006]. Splitting results can be interpreted by (i) correlation with surface geological features considering past and present orogenic activity, (ii) correlation with surface deformation as estimated from GPS, shallow earthquake, and fault activity [e.g., *Flesch and Bendick*, 2012], and (iii) comparison with asthenospheric mantle flow or APM, or any combination thereof [e.g., *Fouch and Rondenay*, 2006]. Moreover, the contribution of crustal anisotropy to teleseismic shear wave splitting is a matter of debate: traditionally regarded as generating delay times approximately a factor of 5 less than mantle anisotropy, several studies argue for significant crustal anisotropy [*Okaya et al.*, 1995; *Wölbern et al.*, 2014]. Shear wave splitting has also been observed in strike-slip regimes where the fast direction tends to align with the strike of the fault [e.g., *Savage*, 1999].

Madagascar is located in the Indian Ocean, with the surrounding major tectonic spreading centers, the East African Rift and the mid-ocean Indian ridge, more than 1000 and 2000 km away, respectively. Commonly, Madagascar is assumed to be part of the Somalian plate. However, recent studies suggest that Madagascar may be traversed by a diffuse plate boundary, separating the Somalian plate from the Lwandle plate [*Kusky et al.*, 2010; *Stamps et al.*, 2008, 2014] (see Figure 1). Moderate seismicity occurs mostly in the central and northern parts, where the focal mechanisms of the larger events mostly indicate ongoing EW extension [*Bertil and Regnoult*, 1998; *Rindraharisaona et al.*, 2013]. The Malagasy lithosphere is characterized by its complex evolution during the Pan-African orogeny, in which several terranes were amalgamated partly by forming near-vertical shear zones. These might penetrate into and, in fact, be controlled by the upper mantle [*Pili et al.*, 1999] (see chapter 2 for details).

In the immediate vicinity of Madagascar, shear wave splitting has been observed on the Seychelles and in the Indian Ocean [*Hammond et al.*, 2005; *Barruol and Fontaine*, 2013]. Both studies relate the observed shear wave splitting to anisotropy caused by a combination of mantle flow due to plate motion and density-driven flow

associated with the African superswell. Lateral variations in the viscosity of the mantle may be necessary to account for regional differences. Anisotropy might also result from flow caused by the interaction of a mantle plume and the lithosphere beneath La Réunion [*Barruol and Fontaine*, 2013] and Seychelles [*Hammond et al*., 2005]. Additionally, *Hammond et al*.'s data set suggests an additional shallow source for anisotropy associated with the separation of the Seychelles from India and Madagascar.

In the study presented here, we examine data from a temporary seismic network and one permanent station, which span the whole width of southern Madagascar and cross its major tectonic provinces. Teleseismic core phases are used to infer seismic anisotropy. We employ a full-waveform modeling approach which will help to characterize the anisotropic properties of the lithosphere and sublithospheric mantle. We test several hypotheses regarding the depth and strength of anisotropy for which we investigate the influence of absolute plate motion, global mantle flow models, and, on a lithospheric scale, the imprint of the shear zones and fossil anisotropy. These results improve our general understanding of geologically complex regions such as Madagascar in the context of past and current kinematics.

2. Geological Setting

Being at the center of, first, the collision between east and west Gondwana and, second, the multistage breakup of Gondwanaland, Madagascar's lithosphere is characterized by different tectonic blocks whose contact zones are defined by suture, shear, and rift zones: the closure of the Mozambique Channel in the Neoproterozoic (~700–800 Ma) was followed by the accretion of terranes and collision of east and west Gondwana during the Pan-African orogeny [*Stern*, 1994; *de Wit*, 2003]. This gave rise to the East African orogeny spanning across Eastern Africa, Madagascar, southern India, Sri Lanka, and coastal Antarctica. In Madagascar, the continent-continent collision was accommodated by crustal thickening and uplift, and the development of near-vertical shear zones [*Stern*, 1994]. Rifting commenced in several stages starting ~300 Ma, with Madagascar finally breaking away from continental Africa during the Jurassic, followed by separation from India/Antarctica at ~90 Ma [*de Wit*, 2003].

Today, the eastern two thirds of the island expose mainly Precambrian rocks. The oldest, Archean-aged rocks can be found in the Antongil block in the northeast and east of the island (Figure 1) which has been interpreted as the outer parts of the Indian Dharwar craton [e.g., *Collins and Windley*, 2002; *Bertil and Regnoult*, 1998]. To the west, the high-grade metamorphic rocks of the Antananarivo block were thermally and structurally reworked during the Neoproterozoic and Early Cambrian [*Collins and Windley*, 2002]. West of the Antananarivo block several also highly strained tectonic units can be differentiated from east to west: the Itremo-Ikalamavony, the Anosyen, Androyen, and Vohibory domains [e.g., *Tucker et al*., 2014]. The western third of the island features several sedimentary basins which formed during and after multistage rifting (Figure 1). Cretaceous volcanism, associated with the separation from India, mainly occurred along the east coast of Madagascar and locally also within sedimentary basins in the west [*Storey et al*., 1995]. During the Cenozoic, resumed volcanism affected central and northern Madagascar [*Bardintzeff et al*., 2009].

Southern Madagascar features a network of steeply dipping, N-S to NW-SE trending shear zones, which were active during the late stages of the Pan-African orogeny [e.g., *Martelat et al*., 2000; *de Wit et al*., 2001]. In particular, the significance of the so-called Ranotsara shear zone is under much debate. While initially considered as a major terrane boundary by *Katz and Premoli* [1979], this feature has later been regarded to be a continuous 350 km long and 20 km wide sinistral intracrustal strike-slip shear zone crosscutting and displacing N-S trending coherent units and shear zones [e.g., *Martelat et al*., 2000; *Collins and Windley*, 2002]. Because of its NW-SE orientation it has been used widely to reconstruct Madagascar's position within Gondwana before breakup by correlation with manifold shear zones in India and Africa [e.g., *Tucker et al*., 1999; *Müller*, 2000; *Collins and Windley*, 2002]. *Schreurs et al*. [2010], however, argue that this lineament is, in fact, a discontinuous structure with ductile deformation and deflection of tectonic units only in its central part and a southeastward prolongation as a brittle normal fault of Phanerozoic to recent age that partly reactivated ductile structures. They thus prefer to use the more neutral term Ranotsara zone for this composite structure.

3. Data and Method

The SELASOMA experiment (Assembly and breakup of Gondwana SEismological signatures in the Lithosphere/Asthenosphere System Of Southern MAdagascar) was carried out between April 2012 and

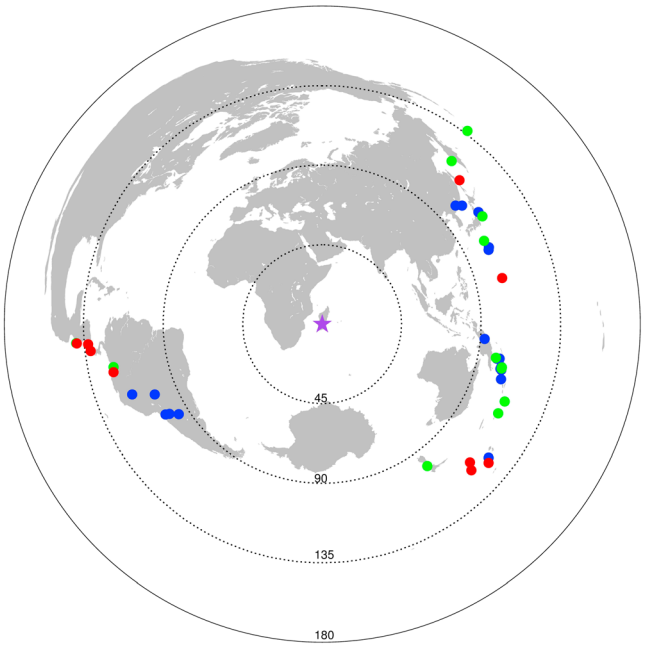

Figure 2. Earthquake distribution for teleseismic phases used in this study. The purple star marks the center of the station profile. Red dots mark events used for splitting analysis at the temporary network and the permanent station. Events only analyzed at the temporary network are marked green, and those at the permanent station are marked blue.

May 2014 [*Tilmann et al*., 2012]. Twenty-five broadband stations were operated on a roughly NE-SW profile, resulting in a linear configuration covering about 530 km with an average station spacing of ~15 km. Twenty-five short-period stations supplemented the profile from April 2013 to May 2014. Additionally, data from the permanent station VOI of the GEOFON network [*GEOFON Data Centre*, 1993] are analyzed between December 2009 and October 2014 (Figure 1). Broadband stations were equipped with 20 Güralp 3ESP and 5 Nanometrics Trillium-240 seismometers using EarthData loggers, whereas Mark L4C-1Hz seismometers and Omnirecs CUBE data loggers were used for the short-period stations. We inspected SKS and SKKS phases of teleseismic events with distances $\geq$85° and PKS phases for distances $\geq$120°, with a magnitude threshold $\geq$6.0 (Figure 2 and supporting information Table S1). This has proven to be a practical limit for having a chance for an acceptable signal-to-noise ratio; we have inspected smaller events at VOI, the permanent station, but none turned out to be usable. We discarded all events from further analysis which did not show a signal-to-noise ratio above 2 and clear onset of the phase. A total of 22 events for the temporary network and 28 events for the permanent station were analyzed, of which 10 were recorded by both. For 42 stations, at least one good quality measurement was obtained. All seismograms were filtered with a bandpass between 0.02 and 0.25 Hz, using a restitution filter on the short-period data first.

Shear wave splitting is analyzed based on the energy-minimization method of *Silver and Chan* [1991]. The initial polarization of the core phases corresponds to the back azimuth [*Long and Silver*, 2009]. Possible misalignments of sensors, including the magnetic declination of ~ −19°, are corrected by estimating the initial polarization from the long-period particle motion [*Rümpker and Silver*, 1998]. Figure 3 shows an example for the single splitting analysis for an event recorded at station AM04. First, North and East components (Figure 3a) are rotated into radial and transverse components (Figure 3b). The initial particle motion is parallel to the back azimuth (red line) for all frequency ranges and displays the expected elliptical form for a split shear wave (Figure 3c). Then a grid search for the splitting parameters δt and Φ which minimize the energy on the transverse component is applied. This is done within a time window initially chosen around the phase, and it is repeated for 50 randomly chosen time windows on the basis of the first chosen time window (Figure 3b). These are used to calculate mean splitting parameters and to check the consistency of the results for single time windows (Figure 3d). If the histogram shows large scatter or a bimodal distribution, the event was discarded as this is indicative of noise or phases contaminated with other phases (for an example, see Figure S1 in the supporting information). We calculate 95% confidence levels (Figure 3e) to estimate the uncertainty of our measurements based on the *F* test [*Silver and Chan*, 1991]. As they overestimate the degrees of freedom by four thirds, which leads to smaller standard errors, we have implemented the corrected equation for the degrees of freedom as shown by *Walsh et al*. [2013].

For split shear waves, the typically elliptical particle motion becomes linear when applying the inverse splitting operator [*Rümpker and Silver*, 1998] to the original waveforms (Figure 3f). If the application of the inverse splitting operator does not lead to the linearization of the particle motion, the event was discarded. Events classified as null measurements show a clear onset of the phase, but no energy on the transverse component.

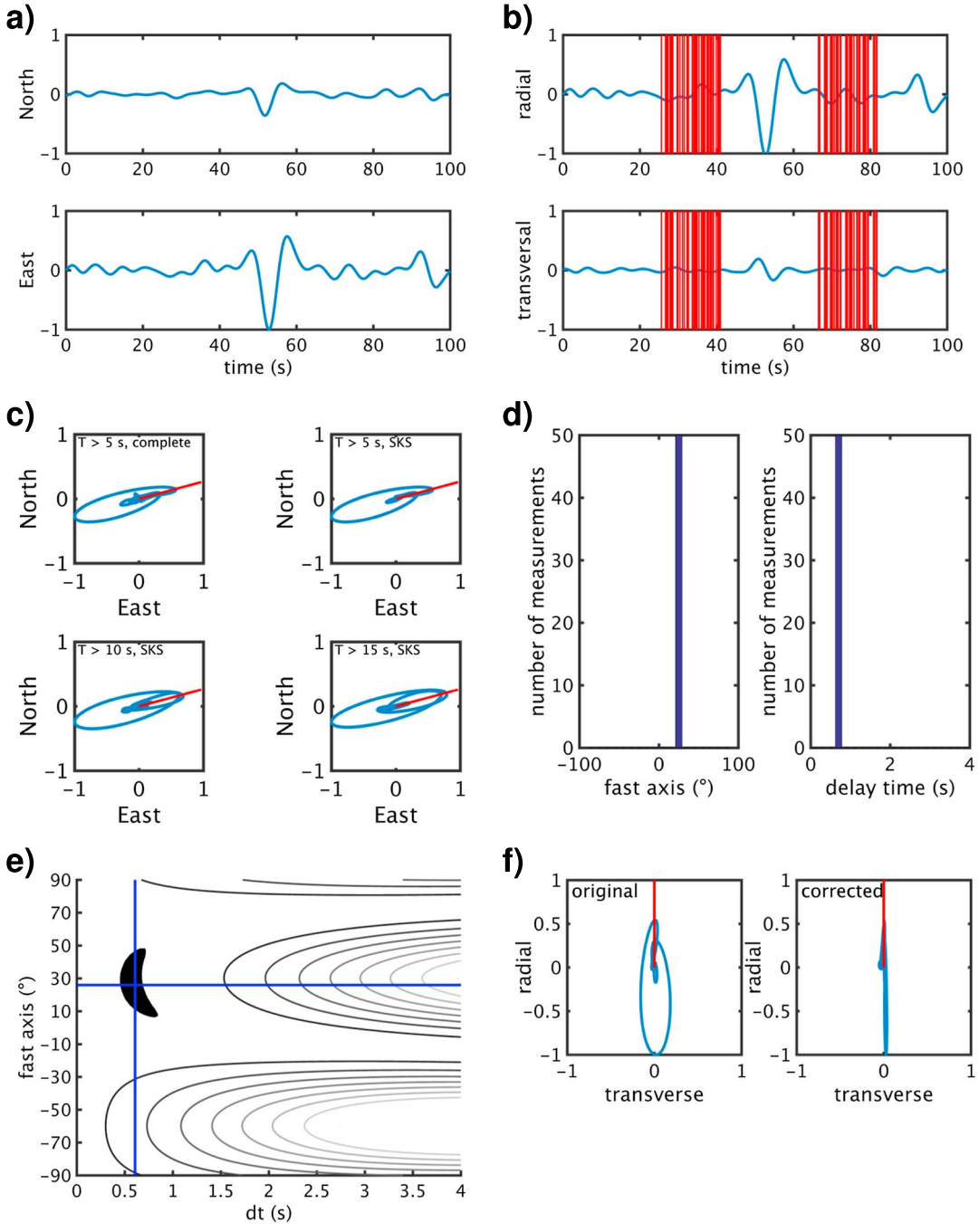

Figure 3. Analysis of an SKS phase recorded at station AM04 of the temporary network. (a) Normalized original North and East components. (b) Normalized radial and transverse components. The red bars denote 50 randomly selected time windows used for the analysis. (c) Particle motions for different periods and time windows. The top left panel corresponds to the entire time window of 100 s. Other panels show the particle motion for a selected time window surrounding the phase of interest (SKS). The red bar indicates the back azimuth. (d) Histogram of splitting parameters for the randomly selected time windows. (e) Energy grid of the corrected transverse component. The blacked contour level refers to the 95% confidence level. The blue cross marks the pair of splitting parameters which minimizes the energy on the transverse component. (f) Original and corrected particle motion plots.

The particle motion is not elliptical but linear even before the application of an inverse splitting operator. Their histogram consequently either shows unusually high delay times and fast directions parallel or perpendicular to the back azimuth, or scattered back azimuths combined with small delay times (for an example of a null measurement, see Figure S2). Single measurements at one given station are usually investigated for the dependence of splitting parameters on back azimuth. Several studies have shown that in the presence of vertically varying anisotropy, e.g., two layers with different anisotropic properties, splitting parameters show a distinct 90° periodicity as a function of back azimuth [e.g., *Savage*, 1999; *Rümpker and Silver*, 1998]. If no such dependence is detected, or azimuthal variations of splitting parameters are insignificant, a single layer of anisotropy is inferred. So-called null measurements can signify the absence of anisotropy altogether or the alignment of the initial polarization of the wave with either the fast or slow axis of the anisotropic layer [*Long and Silver*, 2009].

We apply a joint-splitting analysis as described in *Homuth et al*. [2014] and *Wölbern et al*. [2014] for stations displaying insignificant azimuthal variations. This method utilizes all waveforms at a given station, i.e., including null measurements, and simultaneously minimizes the transverse energy on all components, resulting in one pair of splitting parameters. Waveforms are cut and concatenated so that the sum of the transversal component energy is used in the grid search for the splitting operator which best minimizes the complete transverse component energy. This approach is similar to the energy surface stacking method introduced by *Wolfe and Silver* [1998], but here we work on waveforms directly. Waveforms exhibiting minimal transverse energy (usually resulting in null measurements) may also be included in the joint-splitting analysis. This approach significantly reduces the influence of noise and increases the robustness of the splitting results, thus avoiding overinterpretation of single-phase splitting results. If the used waveforms are inferior in quality or single splitting measurements show significant back azimuthal dependence, the results of the analysis are ambiguous; this is indicated by large scatter in the histogram, and the application of the inverse splitting operator does not lead to a linearization of the particle motions. Figure 4 features an example of a successful joint-splitting measurement for station AM05, which is situated close to the Indian Ocean coast (see Figure S3 for a joint-splitting analysis for a station in the center of the profile). The application of the inverse splitting parameters results in a linearization of the particle motions of all waveforms (Figures 4f–4h), such that it can be concluded that a single layer of anisotropy beneath the station is sufficient to explain the observations. However, in general, this does not exclude the possibility of two-layer splitting.

We developed this approach further by including a grid search over the four parameters that characterize the effects of two anisotropic layers. Hence, we can also apply the joint-splitting method in cases of significant azimuthal variations of the splitting parameters. In the inversion process, the sum of the transverse energy of all phases, which are cut and concatenated, is used. Instead of using a grid search with only one pair of splitting parameters, an inverse splitting operator is calculated from two pairs of splitting parameters, each characterizing the anisotropy in one of the layers. The pair of splitting operators which minimizes the transverse energy is applied to the original waveforms. This should lead to the linearization of particle motion of phases from different back azimuths. Tests with synthetic data demonstrate that this method can recover the different anisotropic properties of a two-layer input model (see supporting information Figure S4). This method requires a good azimuthal distribution, which in Madagascar could only be obtained with the permanent station. A splitting analysis of Ps-converted phases to infer crustal anisotropic parameters [*Rümpker et al*., 2014] was attempted but led to inconclusive results due to the limited azimuthal coverage of receiver functions.

4. Results

From the conventional (single-phase) splitting analysis of core-refracted phases we obtained 101 splitting and 86 null measurements with five stations yielding only one and the remainder on average four to five good measurements. However, in the center of the profile, some stations produced up to 10 good quality measurements. Delay times vary from 0.4 to 1.5 s, with the highest values found at sites near the east coast. On average, a delay time of 0.8 s was obtained, which is just a little below the proposed average of 1 s for continental areas [*Silver and Chan*, 1991]. Figure 5 shows a map of our research area with the results of the single-phase splitting analysis. From west to east, the fast polarizations change from a NE trend to a NNW trend in the center of the profile and change again into a NNE/NE trend toward the Indian Ocean. In the west, results

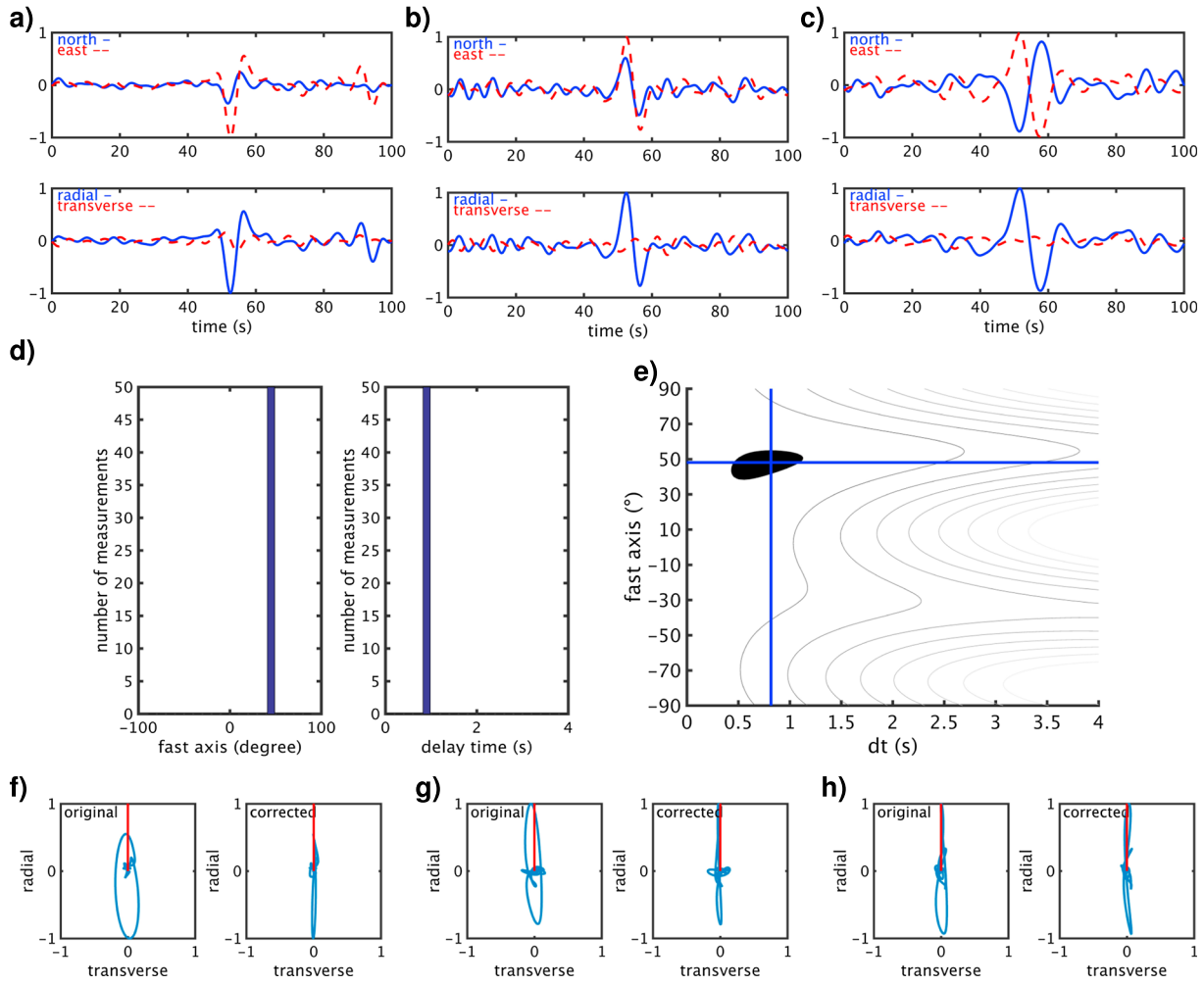

Figure 4. Joint-splitting analysis of shear phases recorded at station AM05. (a–c) North/East (top) and radial/transverse (bottom) components of individual phases. (d) Histogram of splitting parameters for the 50 randomly selected time windows. (e) Grid of the corrected transverse component energy at all three stations. The black contour level refers to the 95% confidence level. The blue cross marks the pair of splitting parameters which minimizes the energy on the transverse components. (f–h) Original and corrected particle motion of the waveforms shown above.

are sparse and the data quality might be hampered by the sedimentary cover, as observed in other shear wave splitting studies [*Kaviani et al*., 2011; *Homuth et al*., 2014]. Fast polarizations in the center of the profile vary at each station but are consistent in their average NNW trend over ~150 km. We note that the scattering of results observed at these stations is not representative of systematic back azimuthal variations. Stations also show null measurements that—as expected—are mostly either approximately parallel to the fast direction of the splitting measurements or perpendicular to that. Toward the Indian Ocean, fast polarizations change to NNE and NE fast-axis directions. As most stations in the east were operating over the period of 1 year only, there are also fewer measurements. Some stations throughout the profile have a number of null measurements from different back azimuths. This might be indicative of a localized, more complex anisotropy beneath those stations, noisy measurements or scattering from heterogeneities, but as neighboring stations do display clear and consistent splitting, we consider the overall pattern to be very robust.

We applied the joint-splitting method (for a single anisotropic layer) to all stations (Figure 6a), as no systematic or periodic variations of splitting parameters with back azimuth could be detected (see supporting information Table S2 for splitting results). Given the small number of single-phase splitting results and their back azimuthal distribution, this does not rule out the presence of two anisotropic layers in general, as we will discuss later. The distinct variations from west to east across the profile are now more clearly visible (see also Figure 6b for splitting parameters along profile). The largest delay times are found within the center of the

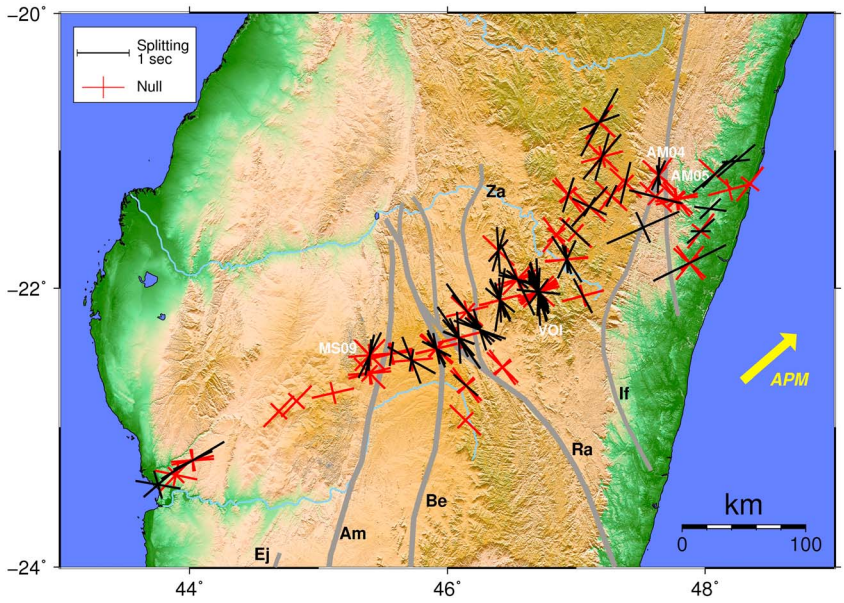

Figure 5. Shear wave splitting results for single-phase splitting analysis. The long axes of the null measurements are plotted parallel to the event BAZ, and the short axis shows the perpendicular direction; fast directions along either one of these directions are compatible with the null measurement. Dashed blue lines are shear zones after *Martelat et al.* [2000]. Ej, Ejeda; Am, Ampanihy; Be, Beraketa; Ra, Ranotsara; Za, Zazafotsy; and If, Ifanadiana.

profile near the Ranotsara zone and along the east coast (Figure 6a). Due to the noisiness of the data in the west, only few stations show clear splitting measurements with NNW aligned fast directions; however, the back azimuths of null measurements and joint-splitting results there are mostly consistent between stations (Figure 6b, marked in green). At station MS09, which is located at the boundary between the Morondava basin and metamorphic basement, the fast axis seems to align with the strike of Ampanihy shear zone (Figures 1 and 6a). In the center of the profile, fast directions are aligned uniformly over 100 km at ~ −30°. To the east of the Ranotsara zone, the change in fast-axis directions occurs over ~100 km. This transition is also marked by three stations without joint-splitting results, where fast axes and null measurements are roughly orthogonal, as denoted in Figure 6b by orange dots. A zone with strong local variations in splitting parameters at ~450 km profile distance forms the eastern part of the transition zone to more uniformly NE-SW oriented fast directions and delay times of just under 1 s in the easternmost part of the study region.

The permanent station VOI of the GEOFON network recorded 28 clear phases. Single splitting measurements show uniform fast axes with three outliers and some null measurements whose back azimuth was perpendicular to the main fast polarization direction. The joint-splitting method reports a fast polarization of −28° (~ ± 4°) and a delay time of 0.6 s (~ ± 0.1 s), where nearly all particle motions are linearized. Subsequently, we applied the joint-splitting approach for two layers, which yielded significantly different estimates for the splitting parameters for different time windows, and the resulting averaged operators also do not lead to a linearization of particle motions. We also calculated apparent splitting parameters for two-layer models based on the equations given in *Silver and Savage* [1994]. The best fitting model is characterized by a lower layer with a fast direction of 70.15° and a splitting delay of 0.8 s and an upper layer with a fast direction of −19.9° and a delay of 1.6 s (Figure 7). However, the fast axes in two layers are very nearly perpendicular to each other, so that for nearly all incoming waves the anisotropy is only seen as one layer with a fast axis of ~ −20° and ~0.8 s. These layer parameters deviate only slightly from the results obtained from the joint-splitting analysis.

5. Modeling

In order to test different plausible models of anisotropy in the mantle and crust beneath the profile, we employ forward modeling to simulate the corresponding waveform effects [see *Homuth et al.*, 2014; *Wölbern et al.*, 2014]. The code used here is based on a finite-difference formulation of the 2-D elastic wave equation [*Rümpker and Ryberg*, 2000] in which the anisotropic properties are defined by an elastic tensor

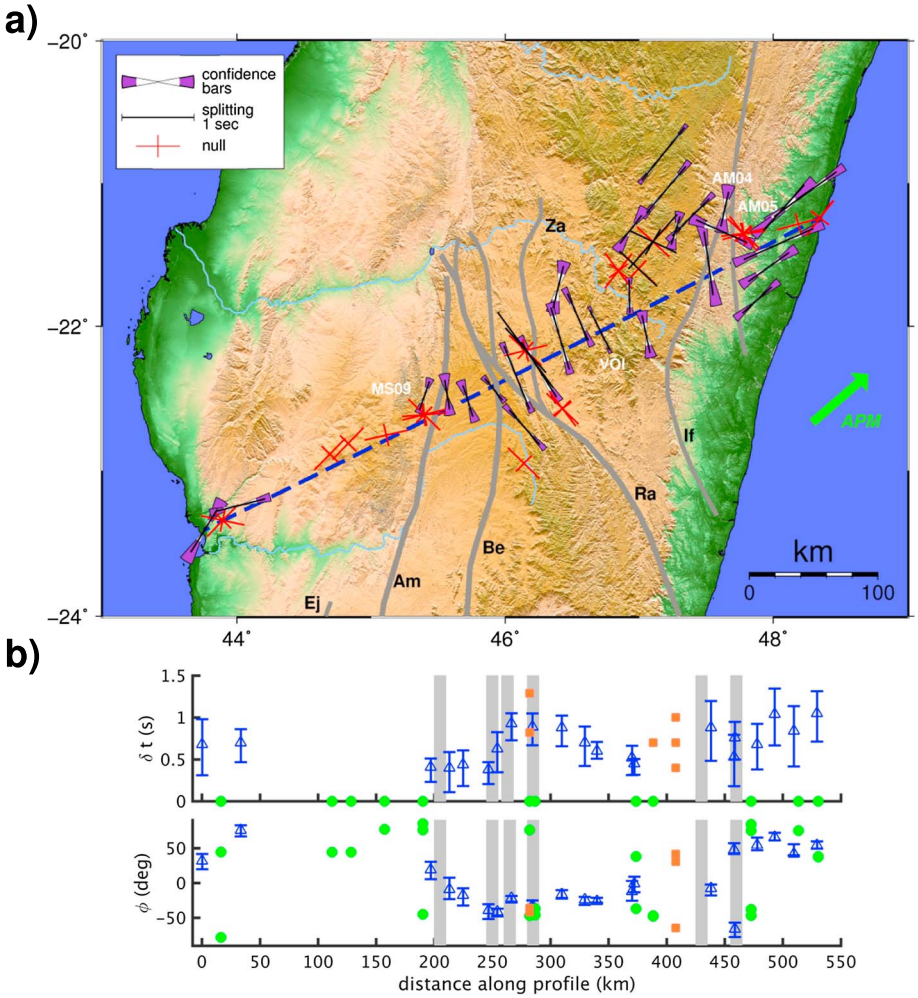

Figure 6. Shear wave splitting results for the joint-splitting analysis. (a) Splitting results are denoted by black bars; null measurements by red crosses where the long axis is parallel to the BAZ. Purple wedges denote the 95% confidence levels. Single splitting results (without underlying wedges) are shown for stations for which the joint-splitting method was not applicable. Dashed blue line marks the profile used in the modeling study, and grey lines are shear zones after *Martelat et al*. [2000]. Ej, Ejeda; Am, Ampanihy; Be, Beraketa; Ra, Ranotsara; Za, Zazafotsy; and If, Ifanadiana. (b) Splitting results along the profile are marked in Figure 6a. Blue triangles represent results from the joint-splitting analysis with error bars indicating the 95% confidence level. Green dots denote back azimuth null measurements. Orange dots denote results of the single splitting analysis, where joint splitting was not applicable. Grey areas represent shear zones. Only measurements for stations less than 40 km away from the main profile are shown here.

exhibiting orthorhombic symmetry. This tensor can be described by nine independent elastic constants, which we set according to the anisotropy of olivine [*Kumazawa and Anderson*, 1969] but scaling down the strength of anisotropy to account for differences in the degree of mineral alignment and the relative abundance of olivine in the mantle. We assume a horizontal *a* axis of the tensor and set the *b* axis to be vertical. Free-surface conditions are applied at the upper boundary of the model, and the grid is chosen to be considerably larger in length and depth than the region of interest to suppress spurious edge effects and to have a vertical and lateral grid spacing of 250 m. If the discretization grid chosen is too wide, waveforms are distorted. Anisotropy due to olivine alignment may extend down to a depth of 400 km, which marks the change from dislocation to diffusion creep [*Fouch and Rondenay*, 2006]. As the vertical resolution of core phases is poor and inferred anisotropy results from a path-integrated measurement [e.g., *Long and Silver*, 2009], we assume that the deepest layer of anisotropy corresponds to the asthenosphere whose maximum depth we set to 200 km. A plane wave is initialized in the isotropic region below and travels as vertical shear wavefront through the model space. At the surface, synthetic horizontal-component seismograms are recorded and the splitting parameters are determined using the single splitting analysis as described above.

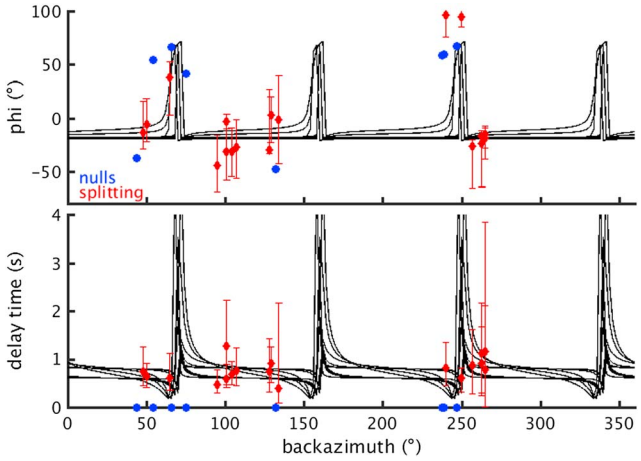

Figure 7. Splitting results for permanent station VOI. Splitting results are plotted in red and null measurements in blue. Black curves, 10 best fitting models from a two-layer minimum misfit calculation.

Synthetic seismograms are calculated for a dominant period of 12 s assuming a vertically incident wavefront, which is suitable for the steeply inclined SKS, SKKS, and PKS phases. We calculate the maximum difference in delay time due to nonvertical incidence to be 2%. The initial polarization is assumed to be oriented at 85°, which due to the 180° periodicity is appropriate for the dominant source regions along the Japan and Marianas trenches as well as for the South American subduction zone (Figure 2), thus encompassing most of the events contributing to the joint-splitting analysis. Furthermore, as the dependence of observed splitting parameters on back azimuth is inconclusive, we refrain from modeling effects of different initial polarizations. For our models, we assume an average crustal thickness of 40 km and an overall lithospheric thickness of 80 km based on seismological [*Rindraharisaona et al*., 2013; *Pasyanos and Nyblade*, 2007] and gravity modeling [*Fourno and Roussel*, 1994]. We compare the splitting results obtained from synthetic and real data, along the profile shown in Figure 6, only using results obtained from stations with a lateral distance to the profile of less than 40 km. For the different models discussed below, we compare the predictions to the observations derived from the joint-splitting analysis. Specific values for the width and strength of anisotropic zones are chosen on the basis of testing a set of plausible choices. The objective is to find an elastic model that predicts splitting parameters that vary in ways similar to those seen in the data. Please see supporting information Text S1 for a detailed explanation of the 2-D finite-difference modeling.

5.1. Single Discrete Shear Zone Versus Ductile Deflected Shear Zone Network

To ascertain which geological interpretation is supported by the results of the splitting analysis, we first consider a single crustal-scale strike-slip shear zone with the approximate dimensions described by *Martelat et al*. [2000]. As the profile crosses the zone at high angle, we use a width of 30 km for the model. For strong deformations, the fast horizontal axis is assumed parallel to the lineation as the strike-slip regime may align the foliation planes vertically. This causes relatively large delay times for shear phases with near-vertical incidence angles [e.g., *Savage*, 1999; *Silver and Chan*, 1991]. For our initial model (Figure 8a, bottom), the lithospheric mantle is set to be isotropic, while we assume 2.8% of anisotropy within the asthenosphere with a fast-axis direction of 50°, which is approximated from the current NNR-MORVEL-56 APM for the Lwandle plate of ~48° (*Argus et al*. [2011], see section 4.2 for further discussion). In the crust, within the shear zone, we assume 12.5% anisotropy and a fast-axis direction of −30°, based on structural directions which vary locally between −30° and −40° (*Martelat et al*. [2000], Figure 8a, bottom). Given the small size of this feature, we find that at least 12% anisotropy is needed to obtain fast polarizations in agreement with our measurements in the center of the profile. Generally, our modeling indicates that variations in the width and strength of the anisotropic features are constrained by about 5 km and 0.25%, respectively. The assumed anisotropic strength is high but not unrealistic for crustal rocks. In the upper crust, anisotropy is thought to be controlled by SPO due to cracks [*Crampin et al*., 1984]. In laboratory experiments, anisotropy of crustal rocks disappears due to the closure of cracks under higher pressure at depths, such as in the middle and lower crusts [*Rasolofosaon et al*., 2000]. Recent findings have shown that amphibole, a main component of the middle to lower crust, can develop significant CPO causing *S* wave anisotropy of 7.6 to 12.1% [*Ko and Jung*, 2015]. In highly anisotropic schists from New Zealand, which were once at lower crustal depths and are now upthrust with near-vertical foliation planes, velocity differences between the fast and slow shear waves of up to 1 km/s were observed [*Okaya et al*., 1995]. The spatial distribution of computed splitting parameters is shown in the two top panels of Figure 8a, denoted by red dots, while observed joint-splitting results are shown as blue triangles with error bars. While delay times and polarization directions obtained from the

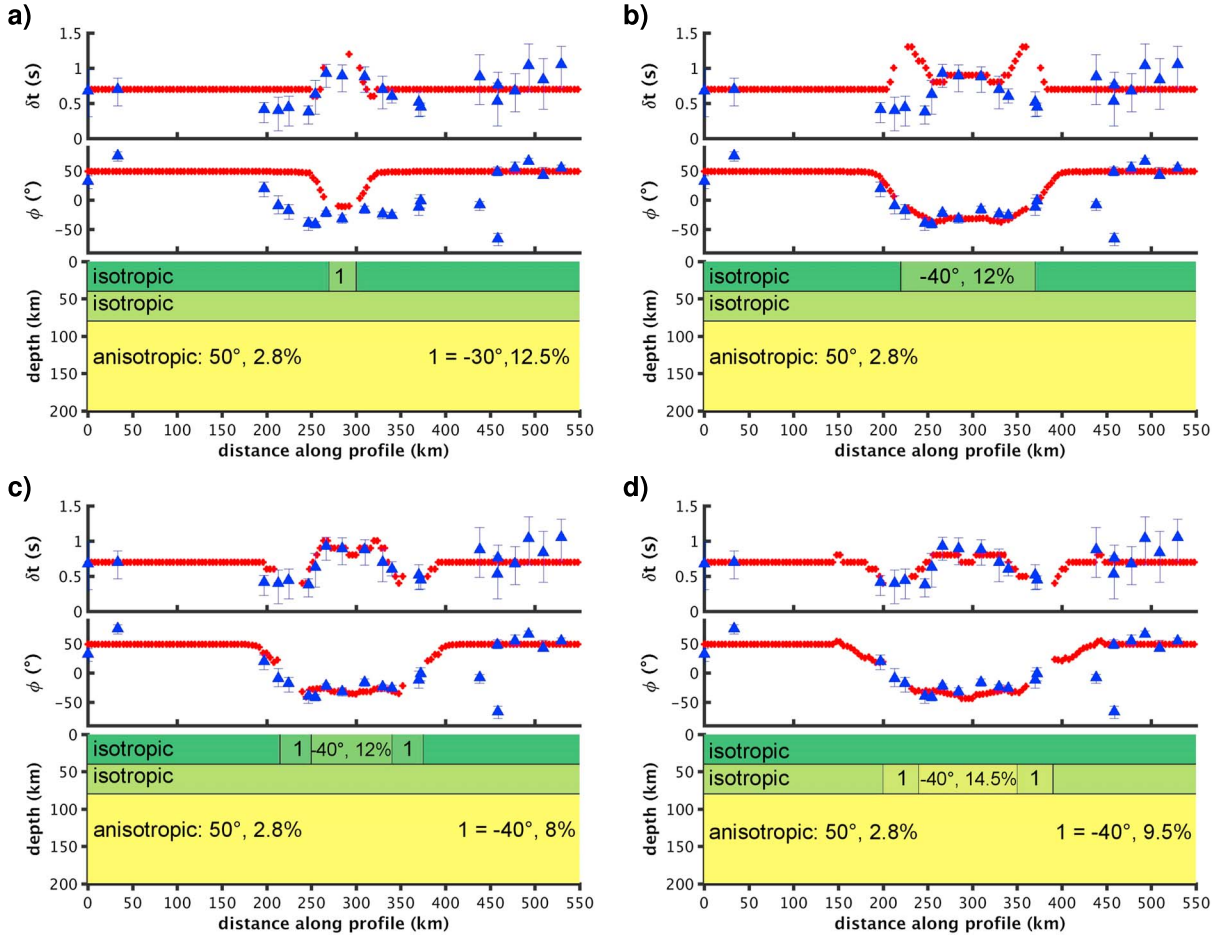

Figure 8. (a–d) Top panels show results of the joint-splitting analysis denoted by blue triangles with error bars. Red dots show the splitting results obtained from finite-difference waveform modeling. Bottom panels show the model used to obtain the synthetic waveforms with fast-axis directions and percent anisotropy. (a) Model characterized by a narrow anisotropic crustal (shear) zone based on geological information. Anisotropy in the asthenospheric mantle is assumed due to APM (MORVEL). (b) Model for distributed ductile shear over a 150 km broad anisotropic zone in the crust. (c) Model for ductile shear distributed over a 150 km broad zone but with reduced anisotropy toward the boundaries. This is our best fit model. (d) Model for a zone of ductile shearing situated only in the lithospheric mantle.

waveform modeling match our observation toward the east and west coasts, this small-scale crustal feature cannot reproduce the orientation and width of change in fast polarization directions around the Ranotsara zone. *Pili et al*. [1999] claim that major shear zones in Madagascar, such as the Ranotsara, are in fact rooted in and controlled by the mantle. Hence, we extend the shear zone down to the lithospheric mantle and change the fast axis to −40°, such that lithospheric and asthenospheric fast directions are orthogonal to each other (supporting information Figure S5). Effectively, the upper layer becomes dominant due to the higher strength of anisotropy and acts virtually as a single layer. However, the shear wave splitting resulting from this model does not exhibit the observed rotation in fast polarization direction over the range of ~150 km.

Next, we examine the contrasting hypothesis that the Ranotsara zone is characterized by ductile bending of deformed tectonic units due to the indentation of the Antananarivo block during continental collision, which should affect the crust and lithosphere over a much wider horizontal range. We assume a ductile deformation zone of crustal anisotropy with a width of 150 km with a fast-axis direction of −40° and 12% anisotropy (Figure 8b). From the comparison between modeling and observations, these values are constrained by about ±0.5%. The asthenospheric anisotropy remains unchanged compared to the previous model. The fast polarization directions predicted by the model agree well with the measurements, except for the outliers at ~450 km, which we will not attempt to accommodate. The rotation of fast polarization is smooth but on a small scale, leading to a good fit of slowly rotating fast directions at the margins of and in the center of

the ductile zone. The model reproduces the delay times in the center of the block of crustal anisotropy but fails to do so at the transition between isotropic and anisotropic crust.

To counter the effect of the abrupt changes in anisotropy to which the delay times seem quite sensitive, we introduce two blocks of reduced crustal anisotropy, each 35 km wide and with 8% anisotropy, with the central block shortened to 90 km lateral extent (Figure 8c, bottom). Modeled splitting results now show a good agreement with the observed splitting parameters. Computed fast polarizations are not significantly altered by the inclusion of additional blocks with reduced anisotropy, while the fit for delay times between ~240 and 340 km along the profile is improved (Figure 8c, top). Projecting the profile onto the geological map, the modeled crustal feature crosses four different tectonic units (Figure 1). Toward the west, this deformation zone is bordered by the sedimentary Morondava basin. In the east, the slow decrease of delay times and change of fast axes roughly coincide with the western margin of the Antananarivo block (Figure 1).

5.2. Distribution of Anisotropy in the Mantle

To study the effects of anisotropy in the mantle lithosphere, we also consider a more conventional model without any crustal anisotropy. A slightly altered, best fitting model is presented in Figure 8d, which consists of a central block of 110 km length, with 14.5% anisotropy, and −40° fast-axis direction. However, based on previous estimates of upper mantle anisotropy from xenolith samples [*Savage*, 1999, and reference therein] such high values of anisotropy may be considered unrealistic. The less anisotropic boundary zones are 40 km wide, each with 9.5% anisotropy and the same fast direction. The changes in anisotropic properties at greater depth result in a less abrupt change of splitting parameters, as can also be derived by the extent of Fresnel zones as a function of depth [*Rümpker and Ryberg*, 2000]. Overall, the model is less suited to explain the steep increase in delay time near profile distance 250 km but does not yield an entirely different result compared to the model with laterally varying crustal anisotropy. Yet it seems unlikely that geologic features and related anisotropic structures manifest themselves in the mantle but not the crust. Exploiting the concept of coherent deformation of the lithosphere in tectonic processes [*Silver and Chan*, 1991], we distribute the crustal feature evenly throughout the entire depth of the lithosphere, effectively reducing the strength of anisotropy to 7% in the central block and to 4.5% in the margins in both crust and lithospheric mantle (Figure S6). The resulting splitting parameters match the majority of observed splitting parameters well. As expected, delay times along the profile change more abruptly in comparison to the previous model but are a little too large at the margins of the deformation zone, while the rotation of fast polarizations matches the splitting results from the joint analysis.

We further examine the possibility of additional blocks of fossil anisotropy in the lithosphere without any underlying anisotropy in the asthenosphere. For our best fitting model, the zone of ductile deformation in the center of the profile is 160 km wide, including the 35 km wide zones of reduced anisotropy on each side (Figure 9a, bottom). Without the underlying asthenospheric anisotropy, we can reduce the strength of anisotropy to 3.85% and 1.6% in the center and the transition zones, respectively, and adjust the fast axes to −30°. East and west of the central and transitional zones, we keep the model as simple as possible and assume a uniform fast-axis direction of 50° and 3.7% anisotropy per layer. Compared to the joint-splitting results, the modeled splitting parameters match the fast polarizations well and just as satisfactorily as the model in Figure 8c. Delay times change smoothly but cannot quite reproduce the abrupt decline or the smallest values at the margins of the deflection zone.

For all previous models with asthenospheric anisotropy, we used an alignment of CPO due to absolute plate motion taken from the NNR-MORVEL-56 plate model [*Argus et al*., 2011], which describes the current motion of 56 plates relative to a no-net-rotation (NNR) reference frame. It includes the Lwandle plate for which it suggests a plate velocity of ~2.7 cm per year. There are other APM models based on different data and assumptions; here we test one directly inferred from 474 published shear wave splitting measurements of cratonic and oceanic interiors [*Kreemer*, 2009]. As such, the inferred anisotropy is thought to constrain the differential motion between lithosphere and mesosphere. The APM model is calculated on the basis of geodetic velocities of relative current plate motions expressed in an NNR model. For Madagascar, an APM of ~33° is derived, though this is based on sparse data; the nearest splitting measurements used were from Mauritius and the Seychelles. We use a simple model with one block of crustal anisotropy with the same width of 150 km as denoted in Figure 8b. Tests have shown that crustal fast axes of −30° or −40° cannot explain the observed splitting parameters in the center of the profile. Here we show a model with a crustal fast axis of −30° and

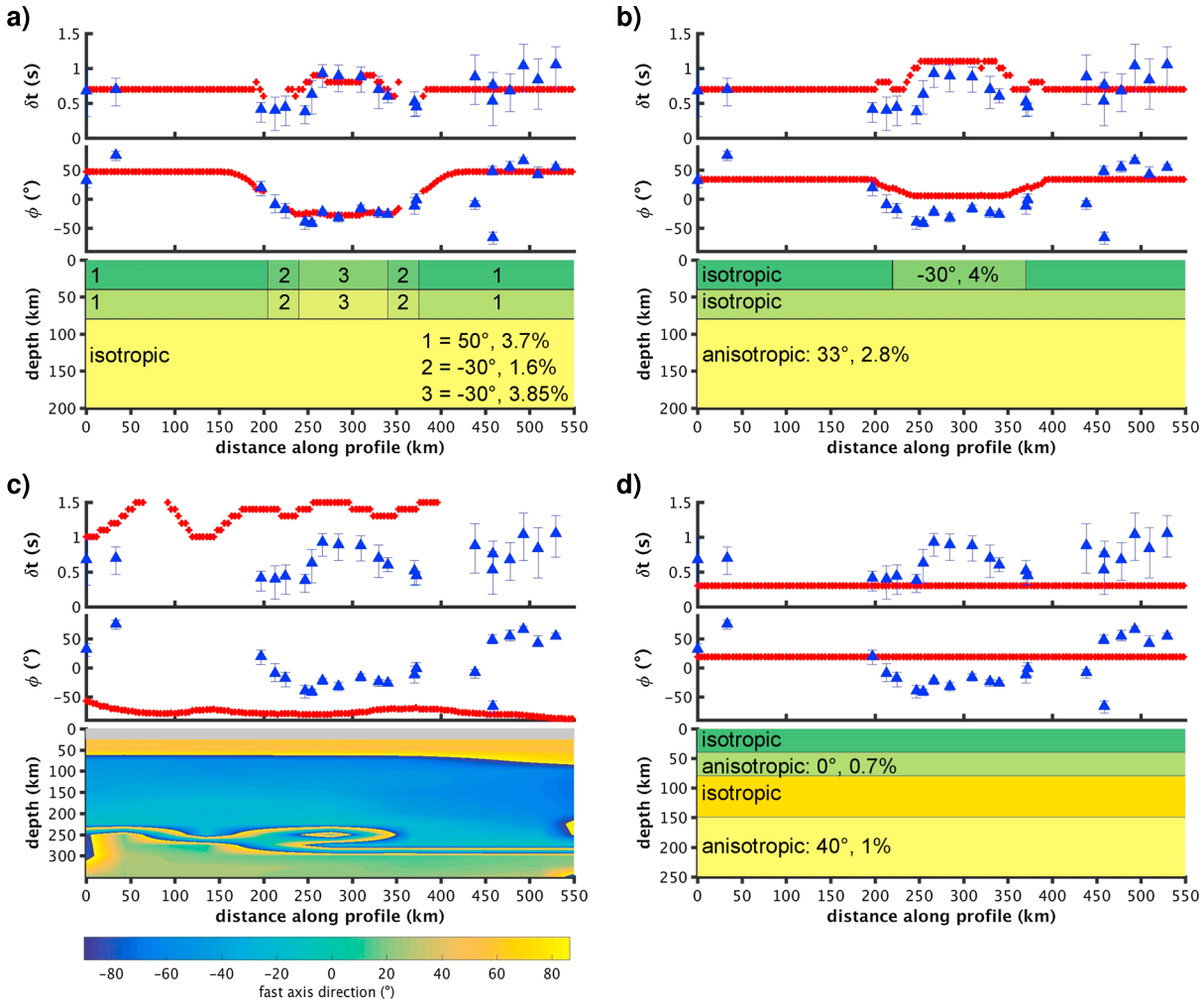

Figure 9. Same as Figure 8 but for different models. (a) Model relying solely on fossil anisotropy in the lithosphere with an isotropic asthenospheric mantle. (b) Zone of ductile shearing in the crust with anisotropy related to APM in the asthenosphere after *Kreemer* [2009]. (c) Mantle flow model after *Miller and Becker* [2012]. (d) Model exhibiting anisotropy patterns derived from surface wave tomography after *Burgos et al.*, 2014.

4% strength of anisotropy, while we assume anisotropy in the asthenosphere of 2.8% and a fast axis of 33° (Figure 9b). Modeled fast polarization directions east and west of the crustal feature divert by ~20° from the observed values. The match between delay times is good except for the smallest values at the transition between isotropic and anisotropic crustal feature. Using a stronger anisotropic crustal layer does not increase the fit to the observed data. As shown in Figure 8c, this could be improved by introducing less anisotropic margins.

5.3. Global Models

In light of recent global studies on anisotropy, we test their applicability for explaining the observed shear wave splitting in Madagascar. First, we construct a model along our profile inferred from the anisotropic properties of the global geodynamic model of *Miller and Becker* [2012], who model mantle flow through density variations as derived from seismic tomography. For our research area in southern Madagascar, their results vary strongly depending on the assumed seismic tomography model and velocity-density conversion, as the region is not as well constrained. Choosing the best-suited model for the study area (T. W. Becker, personal communication, 2015), we use the fast-axis orientation and strength of anisotropy as given by this model along a corridor within 40 km width of our profile as input parameters. Anisotropic parameters from the geodynamic model are specified between 25 and 350 km depth at 14 levels, which we use for interpolation. Accordingly, the crust is set to be isotropic and 25 km thick (Figure 9c, grey area). As the elastic

parameters change on a very fine scale, we plot the fast-axis direction only, as derived from the model of *Miller and Becker* [2012] (please see supporting information Figure S7 for the distribution of strength of anisotropy). The model shows a distinct perturbation of anisotropy below 200 km to the west and center along our profile, implicating complex mantle flow below the asthenosphere, which we have neglected in our previous models so far. However, the strongest anisotropy occurs in a depth range of 25 to 125 km. The delay times vary strongly along the profile and are generally overestimated compared to our results. Fast polarization directions are oriented EW and are at odds with our results.

Finally, we compute a model using the global anisotropic upper mantle surface wave tomographic model of *Burgos et al*. [2014], which is parameterized in terms of fast-axis directions and strength of azimuthal anisotropy in different depth slices, which we use to construct a model with several anisotropic layers. As no data is given for the crust, we assume the crust to be 40 km thick, as before, and isotropic. We use the average of the first two depth slices of the *Burgos et al*. [2014] model to construct a lithospheric anisotropic layer with a fast-axis direction of 0° and 0.7% anisotropy. We use the depth slices between 150 and 250 km to construct an asthenospheric anisotropic layer with an alignment of 40° and 1% anisotropy. By definition this leads to a uniform distribution of splitting parameters along our profile, but the modeled delay times are also generally too small, and modeled and observed fast polarization directions and delay times do not match even outside the region of the zone of ductile deformation.

6. Discussion

In geologically complex areas such as Madagascar, the question arises to what extent the rock fabric (and anisotropy) is preserved in the lithosphere following the extensive deformational past. In general, the role of plate motion and mantle flow must also be considered when interpreting seismic anisotropy. In light of recent findings that Madagascar may be traversed by a diffuse plate boundary separating the Lwandle plate from the Somalian plate [e.g., *Kusky et al*., 2010; *Stamps et al*., 2008], a possible imprint on plate motion and mantle flow needs to be examined. The lateral variations of splitting parameters over relatively short distances along the profile suggest that part of the anisotropic source region is rather shallow [*Rümpker and Ryberg*, 2000]. Splitting parameters in the proximity of the Ranotsara zone align with the strike of the fault, which has been observed previously for other strike-slip regimes [e.g., *Savage*, 1999] and thus appears to support the more traditional interpretation of the Ranotsara zone as a discrete and pure strike-slip shear zone. However, the similarity between splitting parameters toward the east and west coasts also suggests a uniformity of anisotropic properties at greater depth along the profile, possibly reflecting CPO with mantle flow or absolute plate motion.

We have carried out a detailed modeling study in which we test these hypotheses. Using the APM direction for the Lwandle plate for setting the anisotropy direction in the asthenosphere [*Argus et al*., 2011], we first investigate the influence of a discrete, 30 km crustal or lithospheric strike-slip shear zone (Figures 8a and S5). A small scale, localized feature, even if rooted in the mantle, cannot successfully match our data. Hence, our results are not consistent with the hypothesis that the observed shear wave splitting is caused by a single, narrow shear zone. Instead, we achieved the best fit to our splitting measurements using broad blocks of strongly seismically anisotropic crust and lithosphere (Figures 8c and S6). This is consistent with ductile shear deformation distributed over a ~150 km wide zone, affecting parts of the Androyen, Anosyen, and Ikalamavony and Antananarivo domains. The presence of such a wider zone supports the conclusion by *Schreurs et al*. [2010], who find evidence for ductile deflection and distributed deformation of the tectonic units of the Southwestern Madagascar Block (here: Figure 1, units 7–9) through the indentation of the more rigid Antananarivo Block during a late phase of the East African Orogeny ~550–520 Ma ago. Thus, the interpretation of the Ranotsara zone as a terrane separating large-offset shear boundary should be considered with care.

Considering the extensive deformation during the Pan-African orogeny and subsequent separation of Madagascar from surrounding terranes and continents, we also tested to which extent the observed anisotropic patterns could result from fossilized, lithospheric anisotropy only (Figure 8d). Although the fit between modeled and observed splitting parameters is good, we consider this model to be less geologically plausible. Not much is known about the basement units underlying the sedimentary Morondava basin, which could help to infer an alignment of mantle or crustal minerals. To the south of our profile, between 23°S to 25°S and 46°E to ~47°E, *Martelat et al*. [2013] have imaged volcanic dykes using aeromagnetic mapping, which

trend ~30°N. Presumably, anisotropy could be caused by the alignment of melt structures as proposed previously in other regions [*Holtzman and Kendall*, 2010]. If we hypothesize a possible continuation of dykes along their imaged orientation and disregard the 20° deviation from observed splitting parameters, the fossil lithospheric anisotropy hypothesis appears tenable at least in the eastern part. However, there is no reason the same direction should be found in the west of the profile, so that overall an asthenospheric contribution to the seismic anisotropy seems to be the most straightforward interpretation.

Positioning Madagascar in a wider framework, we considered the results of the shear wave splitting analysis with regard to global models. Using Madagascar's position in the Indian Ocean, we first tested the fit between observed and modeled splitting parameters using an alternative APM direction derived from Kreemer's model [2009] (Figure 9b). It assumes that anisotropy at depth is controlled by the shearing of the lithosphere over the mesosphere, which is directly observed though shear wave splitting measurements from, e.g., oceanic plates. The closest measurements to Madagascar are used from the Seychelles and Mauritius, which are, together with Madagascar, allocated to the Somalian plate, neglecting the Lwandle plate. Our calculated model shows a pronounced mismatch for the fast-axis direction of ~20° to observed splitting parameters. If fast polarization directions outside the ductile zone reflect plate kinematics as argued above, arguably the classic techniques of plate motion determination [*Argus et al*., 2011] are superior for predicting the observed splitting patterns far from previous splitting measurement sites.

Furthermore, we examined the coherence between large-scale mantle flow models such as *Miller and Becker* [2012], and seismic tomography presented by *Burgos et al*. [2014], and our data. The prediction of seismic anisotropy from global models and observed splitting measurements often yields significant correlation in oceanic areas, such as the Indian Ocean [*Barruol and Fontaine*, 2013]. They attributed anisotropy beneath the western part of the Indian Ocean to result from a combination of deep mantle convection driven by the South African superswell and small-scale upper mantle heterogeneities caused by an interaction between a mantle plume and the bottom of the lithosphere. As the computed splitting results from models by *Miller and Becker* [2012] (Figure 9c) do not match our data, we infer that deep mantle convection does not seem to control the anisotropic patterns in southern Madagascar. The computed model based on the surface wave tomography model of *Burgos et al*. [2014] also displays a significant misfit between observed and modeled splitting measurements, though the lower layer only deviates by ~10° from the previously inferred APM parallel anisotropy. However, less raypath coverage in the Southern Hemisphere and a generally lower lateral resolution of surface waves might inhibit a closer correlation to splitting results observed in this study. This corroborates previous findings that the resolution of global models of seismic anisotropy from surface wave studies might be insufficient to understand complex continental interiors and is primarily applicable to oceanic interiors. Additionally, we cannot observe or quantify an imprint of a diffuse plate boundary on the observed splitting measurements or the global models regarding mantle flow available at the time. Additional data may be necessary to carefully study the effects of early breakup and their relationship to seismic anisotropy.

As demonstrated with our modeling (Figures 9b–9d), the small-scale rotation of splitting parameters along our profile cannot be matched with the global mantle flow model we tested. We can compute several models involving crustal anisotropy which display a satisfactory fit to the data. However, taking into account geological constraints, we conclude that a crustal or lithosphere scale feature with smoothly changing anisotropic properties best characterizes our observations in the central part of the profile. This could be caused by mineral alignment through ductile flow in the lower crust or lithosphere during the East African orogeny, e.g., caused by the type II or type III alignment of amphibole in the direction of flow as suggested by *Ko and Jung* [2015] for intermediate to high temperatures or stress. The anisotropy in the asthenosphere is likely to result from CPO of olivine in the APM direction in response to shear induced in the asthenosphere by the lithospheric motion.

7. Conclusions

In the study presented here, we employed shear wave splitting measurements to constrain anisotropic patterns beneath southern Madagascar, which are interpreted in terms of the relationship between mantle flow and possibly fossil tectonic processes. Using a dense station profile which crosses the island from the Mozambique Channel to the Indian Ocean, traversing different tectonic units and contact zones, we observe

relatively small-scale variations of splitting parameters. Delay times vary between 0.4 and 1.5 s, and fast polarizations rotate west to east from NNE to NNW and NNE, with minor azimuthal variations such that multiple layers of anisotropy cannot be resolved. Based on full-waveform modeling, we conclude that the observed splitting parameters can be fit by a block of fossil anisotropy with a fast axis of −40° located within the crust or the entire lithosphere. The anisotropy in the asthenosphere reflects current plate motion with an azimuth of ~50° (after NNR-MORVEL 56). The anisotropic properties near the center of our profile are consistent with fossilized CPO due to ductile deformation following the indentation of the more rigid Antananarivo block into the predominantly metasedimentary southern units of Madagascar. A discrete narrow shear zone of 30 km thickness, even when crosscutting the entire lithosphere, cannot by itself explain the observed splitting measurements over a broader ~150 km range at the surface.

Our results further show that models of purely fossilized anisotropy confined to the lithosphere could theoretically explain the splitting observations; however, these would require coincidental alignment of lithospheric fabric with the APM direction, for which there is no convincing geological evidence. Other predictions of APM such as those presented by *Kreemer* [2009], who uses shear wave splitting to constrain absolute plate motion, do not adequately reproduce our observed splitting parameters.

Recently proposed global models of mantle flow based on density heterogeneities, derived from seismic tomography [*Miller and Becker*, 2012; *Burgos et al*., 2014], also do not explain the splitting parameters observed along our profile. Although they might readily be applicable to oceanic basins, in the case of Madagascar with its complex continental interior, they fail to predict the observed anisotropic pattern. Therefore, contributions from lithospheric and especially crustal anisotropy in postcollisional regimes, which is preserved over time as frozen-in fabric, are required to explain the observations.

Acknowledgments
This study was supported by Deutsche Forschungsgemeinschaft (DFG). The fieldwork was funded by GeoForschungsZentrum (GFZ) Potsdam and was conducted together with the Institute and Observatory of Geophysics Antananarivo, Madagascar. We appreciate the fieldwork by all those involved. Instruments were kindly provided by the Geophysical Instrument Pool Potsdam (GIPP), and data were archived by GEOFON [*GEOFON Data Centre*, 1993] and can be accessed at DOI: 10.14470/MR7567431421 [*Tilmann et al*., 2012]. We thank an anonymous reviewer, the Associate Editor, and Martha Savage for constructive comments and suggestions. Ingo Wölbern and Benjamin Homuth are thanked for fruitful discussions and comments on an earlier version of the manuscript. Maps were visualized with the GMT software [*Wessel and Smith*, 1998].

References

Argus, D. F., R. G. Gordon, and C. DeMets (2011), Geologically current motion of 56 plates relative to the no-net-rotation reference frame, *Geochem. Geophys. Geosyst.*, *12*, Q11001, doi:10.1029/2011GC003751.
Bardintzeff, J.-M., J.-P. Ligeois, B. Bonnin, H. Bello, and G. Rasmimanana (2009), Madagascar volcanic provinces linked to the Gondwana break-up: Geochemical and isotopic evidences for contrasting mantle sources, *Gondwana Res.*, *18*, 295–315, doi:10.1016/j.gr.2009.11.010.
Barruol, G., and F. R. Fontaine (2013), Mantle flow beneath La Réunion hotspot track from SKS splitting, *Earth Planet. Sci. Letters*, *362*, 108–121, doi:10.1016/j.epsl.2012.11.017.
Becker, T. W., C. P. Conrad, A. J. Schaeffer, and S. Lebedev (2014), Origin of azimuthal seismic anisotropy in oceanic plates and mantle, *Earth Planet. Sci. Letters*, *401*, 236–250, doi:10.1016/j.epsl.2014.06.014.
Bertil, D., and J. M. Regnoult (1998), Seismotectonics of Madagascar, *Tectonophysics*, *294*, 57–74.
Bésairie, H. (1971), *Tectonique de Madagascar, Tectonique de l' Afrique*, pp. 549–558, Sciences de la Terre UNESCO, Paris.
Burgos, G., J.-P. Montagner, E. Beucler, Y. Capdeville, A. Mocquet, and M. Drilleau (2014), Oceanic lithosphere-asthenosphere boundary from surface wave dispersion data, *J. Geophys. Res. Solid Earth*, *119*, 1079–1093, doi:10.1002/2013JB010528.
Crampin, S., E. M. Chesnokovet, and R. G. Hipkin (1984), Seismic anisotropy—The state of the art: II, *Geophys. J. Roy. Astron. Soc.*, *76*, I–16.
Collins, A. S., (2000), The Tectonic Evolution of Madagascar: Its Place in the East African Orogen, *Gondwana Res.*, *3*(4), 549–552.
Collins, A. S., and B. F. Windley (2002), The tectonic evolution of central and northern Madagascar and its place in the final assembly of Gondwana, *J. Geology*, *110*, 325–339.
de Wit, M. J., S. A. Bowring, L. D. Ashwal, L. G. Randrianasolo, and V. P. I. Morel (2001), Age and tectonic evolution of Neoproterozoic ductile shear zones in southwestern Madagascar, with implications for Gondwana studies, *Tectonics*, *20*, 1–45, doi:10.1029/2000TC900026.
de Wit, M. J. (2003), Madagascar: Heads it's a continent, tails it's an island, *Annu. Rev. Earth Planet. Sci.*, *31*, 213–48, doi:10.1146/annurev.earth.31.100901.141337.
Flesch, L., and R. Bendick (2012), The relationship between surface kinematics and deformation of the whole lithosphere, *Geology*, *40*, 711–714.
Fouch, M. J., and S. Rondenay (2006), Seismic anisotropy beneath stable continental interiors, *Phys. Earth Planet. Inter.*, *158*, 292–320, doi:10.1016/j.pepi.2006.03.024.
Fourno, J.-P., and J. Roussel (1994), Imaging of the Moho depth in Madagascar through the inversion of gravity data: Geodynamic implications, *Terra Nova*, *6*, 512–519.
GEOFON Data Centre (1993), GEOFON seismic network (GE), Deutsches GeoForschungsZentrum GFZ, seismic network, doi:10.14470/TR560404.
Hammond, J. O. S., J.-M. Kendall, G. Rümpker, J. Wookey, N. Teanby, P. Joseph, T. Ryberg, and G. Stuart (2005), Upper mantle anisotropy beneath the Seychelles microcontinent, *J. Geophys. Res.*, *110*, B11401, doi:10.1029/2005JB003757.
Holtzman, B. K., and J. M. Kendall (2010), Organized melt, seismic anisotropy, and plate boundary lubrication, *Geochem. Geophys. Geosyst.*, *11*, Q0AB06, doi:10.1029/2010GC003296.
Homuth, B., U. Löbl, A. G. Batte, K. Link, C. M. Kasereka, and G. Rümpker (2014), Seismic anisotropy of the lithosphere/asthenosphere system beneath the Rwenzori region of the Albertine Rift, *Int. J. Earth. Sci.*, *105*, 1681–1692, doi:10.1007/s00531-014-1047-0.
Jourde, G. (1971), Essai de synthèse structurale et stratigraphique de Précambrien malgache, Compte Rendu Sociète Géologique Madagascar, pp. 59–69.
Karato, S., and P. Wu (1993), Rheology of the upper mantle: A synthesis, *Science*, *260*, 771–778.
Katz, M. B., and C. Premoli (1979), India and Madagascar in Gondwanaland: a fit based on Precambrian tectonic lineaments, *Nature*, *1791*, 312–315.
Kaviani, A., G. Rümpker, M. Weber, and G. Asch (2011), Short-scale variations of shear-wave splitting across the Dead Sea basin: Evidence for effects of sedimentary fill, *Geophys. Res. Lett.*, *38*, L04308, doi:10.1029/2010GL046464.

Ko, B., and H. Jung (2015), Crystal preferred orientation of an amphibole experimentally deformed by simple shear, *Nat. Commun.*, *6*, 6586, doi:10.1038/ncomms7586.
Kreemer, C. (2009), Absolute plate motions constrained by shear wave splitting orientations with implications for hot spot motions and mantle flow, *J. Geophys. Res.*, *114*, B10405, doi:10.1029/2009JB006416.
Kumazawa, M., and O. L. Anderson (1969), Elastic moduli, pressure derivatives, and temperature derivatives of single-crystal olivine and single-crystal forsterite, *J. Geophys. Res.*, *74*, 5961–5972.
Kusky, T. M., E. Toraman, T. Raharimahefa, and C. Rasoazanamparany (2010), Active tectonics of the Alaotra-Ankay graben system, Madagascar: Possible extension of Somalian-African diffusive plate boundary?, *Gondwana Res.*, *18*(2), 274–294, doi:10.1016/j.gr.2010.02.003.
Long, M. D., and P. G. Silver (2009), Shear wave splitting and mantle anisotropy: Measurements, interpretations, and new directions, *Surv. Geophys.*, *30*, 407–461.
Martelat, J.-E., J.-M. Lardeaux, C. Nicollet, and R. Rakotondrazafy (2000), Strain pattern and Late Precambrian deformation history in southern Madagascar, *Precambrian Res.*, *102*, 1–20.
Martelat, J.-E., B. Randrianasolo, K. Schulmann, J.-M. Lardeaux, and J.-L. Devidal (2013), Airborne magnetic data compared to petrology of crustal scale shear zones from southern Madagascar: A tool for deciphering magma and fluid transfer in orogenic crust, *J. Afr. Earth Sci.*, doi:10.1016/j.jafrearsci.2013.07.003.
Miller, M. S., and T. W. Becker (2012), Mantle flow deflected by interactions between subducted slabs and cratonic keels, *Nat. Geosci.*, *5*, 726–730, doi:10.1038/NGEO1553.
Müller, B.G.J. (2000), The evolution and significance of the Bongolava-Ranotsara shear zone, Madagascar, PhD thesis, Rand Afrikaans University, Johannesburg.
Okaya, D., N. Christensen, D. Stanley, and T. Stern (1995), Crustal anisotropy in the vicinity of the Alpine Fault Zone, N.Z, *J. Geol. Geophys.*, *38*, 579–583.
Pasyanos, M. E., and A. A. Nyblade (2007), A top to bottom lithospheric study of Africa and Arabia, *Tectonophysics*, *444*, 27–44.
Pili, E., S. M. F. Sheppard, and J.-M. Lardeaux (1999), Fluid-rock interaction in the granulites of Madagascar and lithospheric-scale transfer of fluids, *Gondwana Res.*, *2*(3), 341–350.
Rasolofosaon, P. N. J., W. Rabbel, S. Siegesmund, and A. Vollbrecht (2000), Characterization of crack distribution: Fabric analysis versus ultrasonic inversion, *Geophys. J. Int.*, *141*, 413–424.
Rindraharisaona, E. J., M. Guidarelli, A. Aoudia, and G. Rambolamanana (2013), Earth structure and instrumental seismicity of Madagascar: Implications on the seismotectonics, *Tectonophysics*, *594*, 165–181, doi:10.1016/j.tecto.2013.03.033.
Rümpker, G., A. Kaviani, and K. Latifi (2014), Ps-splitting analysis for multilayered anisotropic media by azimuthal stacking and layer stripping, *Geophy. J. Int.*, *199*, 146–163, doi:10.1093/gji/ggu154.
Rümpker, G., and T. Ryberg (2000), New "Fresnel-zone" estimates for shear-wave splitting observations from finite-difference modeling, *Geophys. Res. Lett.*, *27*, 2005–2008, doi:10.1029/2000GL011423.
Rümpker, G., and P. G. Silver (1998), Apparent shear-wave splitting parameters in the presence of vertically-varying anisotropy, *Geophys. J. Int.*, *135*, 790–800.
Savage, M. K. (1999), Seismic anisotropy and mantle deformation: What have we learned from shear wave splitting?, *Rev. Geophys.*, *37*, 65–106 , doi:10.1029/98RG02075.
Schreurs, G., J. Giese, A. Berger, and E. Gnos (2010), A new perspective on the significance of the Ranotsara shear zone in Madagascar, *Int. J. Earth Sci.*, *99*, 1827–1847, doi:10.1007/s00531-009-0490-9.
Silver, P. G., and W. Chan (1991), Shear wave splitting and subcontinental mantle deformation, *J. Geophys. Res.*, *96*, 16,429–16,454, doi:10.1029/91JB00899.
Silver, P. G., and M. K. Savage (1994), The interpretation of shear-wave splitting parameters in the presence of two anisotropic layers, *Geophys. J. Int.*, *119*, 949–963.
Stamps, D. S., E. Calais, S. Elifuraha, C. Hartnady, J.-M. Nocquet, C. J. Ebinger, and R. M. Fernandes (2008), A kinematic model for the East African Rift, *Geophys. Res. Let.*, *35* L05304, doi:10.1029/2007GL032781.
Stamps, D. S., L. M. Flesch, E. Calais, and A. Ghosh (2014), Current kinematics and dynamics of Africa and the East African Rift System, *J. Geophys. Res. Solid Earth*, *119*, 5161–5186, doi:10.1002/2013JB010717.
Stern, R. J. (1994), Arc assembly and continental collision in the Neoproterozoic East African orogen, *Annu. Rev. Earth Planet. Sci.*, *22*, 319–351.
Storey, M., J. J. Mahoney, A. D. Saunders, R. A. Duncan, S. P. Kelley, and M. F. Coffin (1995), Timing of hot spot-related volcanism and the breakup of Madagascar and India, *Science*, *267*, 852–855, doi:10.1126/science.267.5199.852.
Tilmann, F., X. Yuan, G. Rümpker, and E. Rindraharisaona (2012), SELASOMA Project, Madagascar (ZE 2012-2014), Deutsches GeoForschungsZentrum GFZ, Seismic Network, doi:10.14470/MR7567431421.
Tucker, R. D., J. Y. Roig, B. Moine, C. Delor, and S. G. Peters (2014), A geological synthesis of the Precambrian shield in Madagascar, *J. Afr. Earth Sci.*, *94*, 9–30.
Tucker, R. D., L. D. Ashwal, M. J. Handke, M. A. Hamilton, M. LeGrange, and R. A. Rambeloson (1999), U-Pb geochronology and isotope geochemistry of the Archean granite-greenstone belts of Madagascar, *J. Geol.*, *107*, 135–153.
Walker, K. T., A. A. Nyblade, S. L. Klemperer, G. H. R. Bokelmann, and T. J. Owens (2004), On the relationship between extension and anisotropy: Constraints from shear-wave splitting across the East African plateau, *J. Geophys. Res.*, *109*, B08302, doi:10.1029/2003JB002866.
Walsh, E., R. Arnold, and M. K. Savage (2013), Silver and Chan revisited, *J. Geophys. Res. Space Physics*, *118* 5500-5515, doi:10.1002/jgrb.50386.
Wessel, P., and W. H. F. Smith (1998), New, improved version of the Generic Mapping Tools released, *Eos. Trans. AGU*, *79*, 579, doi:10.1029/98EO00426.
Wolfe, C. J., and P. G. Silver (1998), Seismic anisotropy of oceanic upper mantle: Shear-wave splitting methodologies and observations, *J. Geophys. Res.*, *103*, 749–771, doi:10.1029/97JB02023.
Wölbern, I., U. Löbl, and G. Rümpker (2014), Crustal origin of trench-parallel shear wave fast polarizations in the Central Andes, *Earth Planet. Sci. Lett.*, *392*, 230–238, doi:10.1016/j.epsl.2014.02.032.